



A Journal of the Gesellschaft Deutscher Chemiker

Angewandte Chemie

GDCh

International Edition

www.angewandte.org

Accepted Article

Title: Slipped Structure of Covalent Organic Framework Facilitates Two-Photon Adsorption for Improving Near-Infrared Excited Fluorescence Imaging

Authors: Jin-Yue Zeng, Xiao-Shuang Wang, Bo-Ru Xie, Min-Jie Li, and Xian-Zheng Zhang

This manuscript has been accepted after peer review and appears as an Accepted Article online prior to editing, proofing, and formal publication of the final Version of Record (VoR). This work is currently citable by using the Digital Object Identifier (DOI) given below. The VoR will be published online in Early View as soon as possible and may be different to this Accepted Article as a result of editing. Readers should obtain the VoR from the journal website shown below when it is published to ensure accuracy of information. The authors are responsible for the content of this Accepted Article.

To be cited as: *Angew. Chem. Int. Ed.* 10.1002/anie.201912594
Angew. Chem. 10.1002/ange.201912594

Link to VoR: <http://dx.doi.org/10.1002/anie.201912594>
<http://dx.doi.org/10.1002/ange.201912594>

Slipped Structure of Covalent Organic Framework Facilitates Two-Photon Adsorption for Improving Near-Infrared Excited Fluorescence Imaging

Jin-Yue Zeng,^[a] Xiao-Shuang Wang,^[a] Bo-Ru Xie,^[a] Min-Jie Li,^[a] and Xian-Zheng Zhang^{[a,b]*}

Abstract: Fluorescent materials exhibiting the characteristics of strong two-photon absorption (TPA) are extensively used for nonlinear optics, bio-imaging and phototherapy. One practical approach to obtain fluorescent materials with high TPA performance is to polymerize molecular chromophores to form π -conjugated structure. This leads to the increase in TPA cross-section per chromophore, however, efforts to towards this direction was capped by the lack of long-range ordering in the structure and the strong π - π stacking between the chromophores. Here, we reported the rational design of benzothiadiazole-based covalent organic framework (COF) for promoting TPA performance and obtaining the efficient two-photon excited fluorescence. Structure characterizations and spectroscopic studies revealed that the enhancement in TPA performance was attributed to the donor- π -acceptor- π -donor (D- π -A- π -D) configuration of the chromophore, long-range order, and large π -conjugation domain of COF crystals. The structural slipping in TPA-COF not only attenuates the π - π stacking interaction between the layers, but more importantly, overcomes the aggregation-caused emission quenching of the chromophores for improving near-infrared two-photon excited fluorescence imaging.

Introduction

Integrating functional molecules into conjugated crystalline structures represents a fast-developing branch of material science in the past few decades.^[1] Covalent organic frameworks (COFs), constructed by linking organic molecules through covalent bond, are a class of emerging crystalline porous polymer, which exhibit the atomically precise incorporation of organic units into extensible structures with periodic frameworks and ordered nanopores.^[2] Indeed, COFs provide confined molecular spaces for the interaction of photons, excitons, electrons, holes and guest molecules, thereby displaying unique molecular and crystalline features.^[3] The molecular features of these materials allows for the design and tailoring of their pore properties and functionality, providing specific interaction with guest molecules, thus leads to excellent performance in separation, catalysis, molecular recognition and drug delivery.^[4] On the other hand, the crystalline features, involving the long-range ordering between molecular building blocks that restricted

the configuration inversions of the linkers in the lattices and the enforced π -conjugation that ensures the extended delocalization of π -electrons, were much less explored.^[5] These are critical, however, for their electrical, magnetic and optical properties.

Organic conjugated chromophores possessing a large two-photon absorption (TPA) cross-section are of interest for many practical applications, such as nonlinear optics, 3D fluorescence imaging and phototherapy.^[6] The two-photon excitation with near-infrared (NIR) light provides a better definition of less photo-damage, the focal spot and resolution, and deeper penetration in biological tissues compared with general one-photon excitation upon UV and visible light (Figure 1A and 1B).^[7] To facilitate these applications, the development and design of fluorescent materials with efficient TPA performance are essential.^[8] The TPA performance of fluorescent materials is generally determined by their TPA cross-section, which is influenced by the molecule conformation, the transition dipole moment of molecule and π -conjugation domain.^[9] Previous studies indicated that the TPA cross-section can be improved in amorphous polymer by enlarging the π -conjugated domain.^[10] Meanwhile, the increase of TPA cross-section was also found in recent study in metal organic frameworks (MOFs) by incorporating the chromophores into three-dimensional crystal lattices.^[11] These approaches led to the enhancement in TPA cross-section per chromophore, however, efforts to towards this direction was limited by π - π stacking between the chromophores and the lack of long-range ordering in the structure.^[12]

Here, we designed a benzothiadiazole-based COF with slipped structure to promote TPA performance by using donor- π -acceptor- π -donor (D- π -A- π -D) configuration of the chromophores as building blocks, and to achieve the efficient TPA performance for NIR-excited fluorescent materials (Figure 1C and 1D). The promotion of TPA performance was attributed to the following several factors: a) D- π -A- π -D configuration of the chromophores to enhance polarization of the charge distribution.^[13] b) Large π -conjugation domain to ensure effective π -delocalization with strong extended intramolecular charge transfer.^[14a] c) Restriction of intramolecular bond rotation to block the non-radiative energy decay pathway.^[14b] d) Regular intervals of the TPA chromophore in slipped frameworks to avoid unwanted aggregation and concentration quenching.^[15] Because of exploiting the unique nature of COF, the long-range crystal domain and eclipsed π - π stacking structure will be greatly improved with enforced coplanarity conformation which will lead to high dipole value and large TPA cross-section value.^[14a] As a proof-of-concept, the benzothiadiazole-based COF with high TPA activity was used as enhanced fluorescent material for two-photon excited fluorescence imaging *in vitro* and *in vivo* (Figure 1E).

[a] Dr. J.-Y. Zeng, X.-S. Wang, B.-R. Xie, M.-J. Li, Prof. Dr. X.-Z. Zhang
Key Laboratory of Biomedical Polymers of Ministry of Education &
Department of Chemistry, Wuhan University
Wuhan 430072, China
E-mail: xz-zhang@whu.edu.cn
[b] Prof. Dr. X.-Z. Zhang
The Institute for Advanced Studies, Wuhan University
Wuhan 430072, China

Supporting information for this article is given via a link at the end of the document.

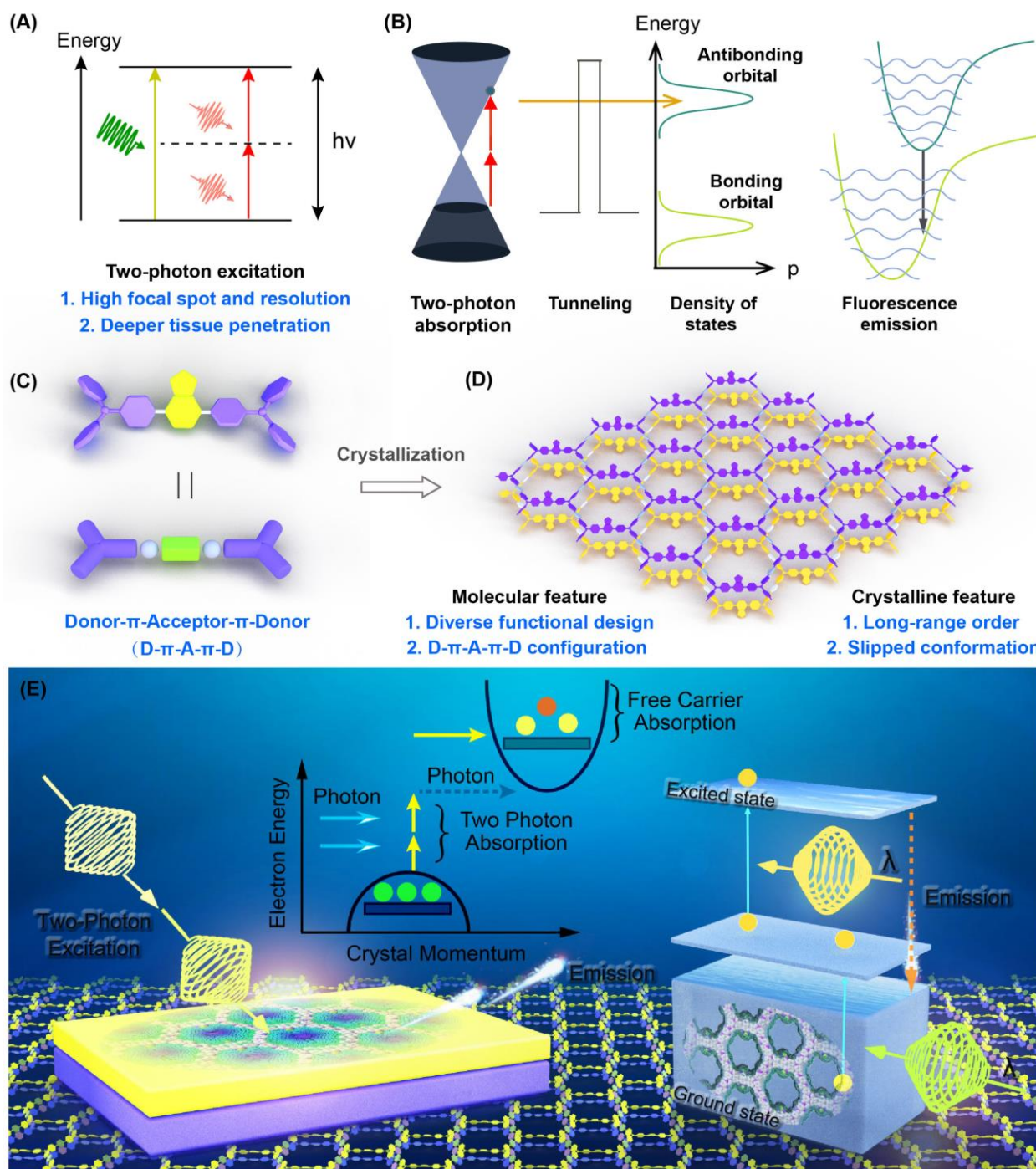


Figure 1. (A) Schematic illustration of one-photon, two-photon excitation and the advantages of two-photon excitation. (B) Schematic illustration of the mechanism of two-photon excited fluorescence emission. (C) The choice of building block with π -acceptor- π -donor (D- π -A- π -D) chromophores. (D) Illustration of the molecular feature and the crystalline feature of COFs. (E) Schematic illustration of TPA-COF facilitates near-infrared excited fluorescence emission (left, the mechanism of two-photon excited fluorescence emission; right, the schematic energy level diagram of two-photon excited fluorescence emission).

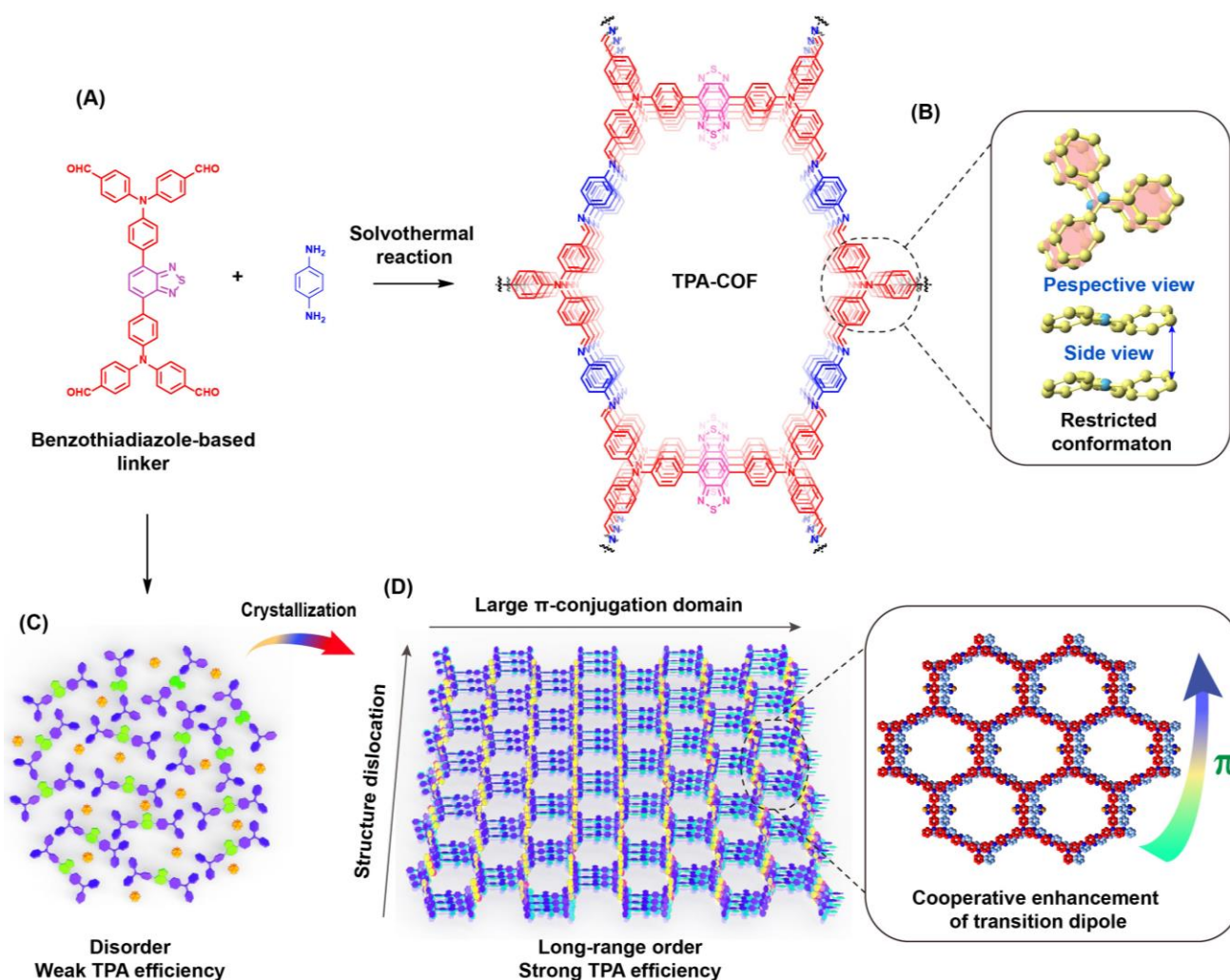


Figure 2. (A) Schematic illustrating the synthesis of TPA-COF. (B) The restricted conformation dynamics in the crystal lattice. (C) The disorder structure induced weak TPA efficiency. (D) Illustration of the long-range ordering coherent domain and the cooperative enhancement of transition dipole in TPA-COF led to strong TPA efficiency.

Results and Discussion

The typical synthesis of COF with TPA (TPA-COF) was achieved by solvothermal reaction of benzothiadiazole-based aldehyde molecular chromophores with aniline building blocks, where the reversibility of the imine linkage guaranteed the formation of COF with high crystallinity, thus led to excellent long-range ordering of the molecular chromophores (Figure 2A-2D). A series of spectroscopic experiments were performed to characterize the structure of TPA-COF. The Fourier transform infrared (FT-IR) spectrum of TPA-COF clearly show the characteristic telescopic vibration of imine bond ($\nu_{C=N}$) at 1612 cm^{-1} , suggesting the formation of the imine linkage (Figure S1). The quantitative conversion of the aldehyde was further confirmed by the cross-polarization magic-angle-spinning ^{13}C solid-state nuclear magnetic resonance (CP/MAS ^{13}C NMR) spectrum. After constructing to COF, the aldehyde carbon peak

belonging to the ligands at 190.6 ppm disappeared completely in the CP/MAS ^{13}C NMR spectrum, and a new peak at 158.7 ppm emerged, indicating the quantitative formation of imine linkages (Figure S2 and S3). The porosity of TPA-COF was investigated by measuring N_2 adsorption-desorption at 77 K exhibited a rapid uptake at a low pressure of $P/P_0 < 0.1$, followed by a sharp step between $P/P_0 = 0.1$. The Brunauer-Emmett-Teller (BET) surface areas of TPA-COF is found to be $1030\text{ m}^2\text{ g}^{-1}$ indicating that TPA-COF has good to porosity (Figure S4). The morphology of TPA-COF was examined by both scanning electron microscopy (SEM) and transmission electron microscopy (TEM), where the COF exhibited uniform layered structures with ordered shapes (Figure 3A and 3B). The elemental mapping of C, N, O and S in a single TPA-COF showed geometrical and compositional distributions (Figure 3E). These results indicated that a porous polymer was constructed by linking benzothiadiazole-based aldehyde with aniline building blocks through covalent bond.

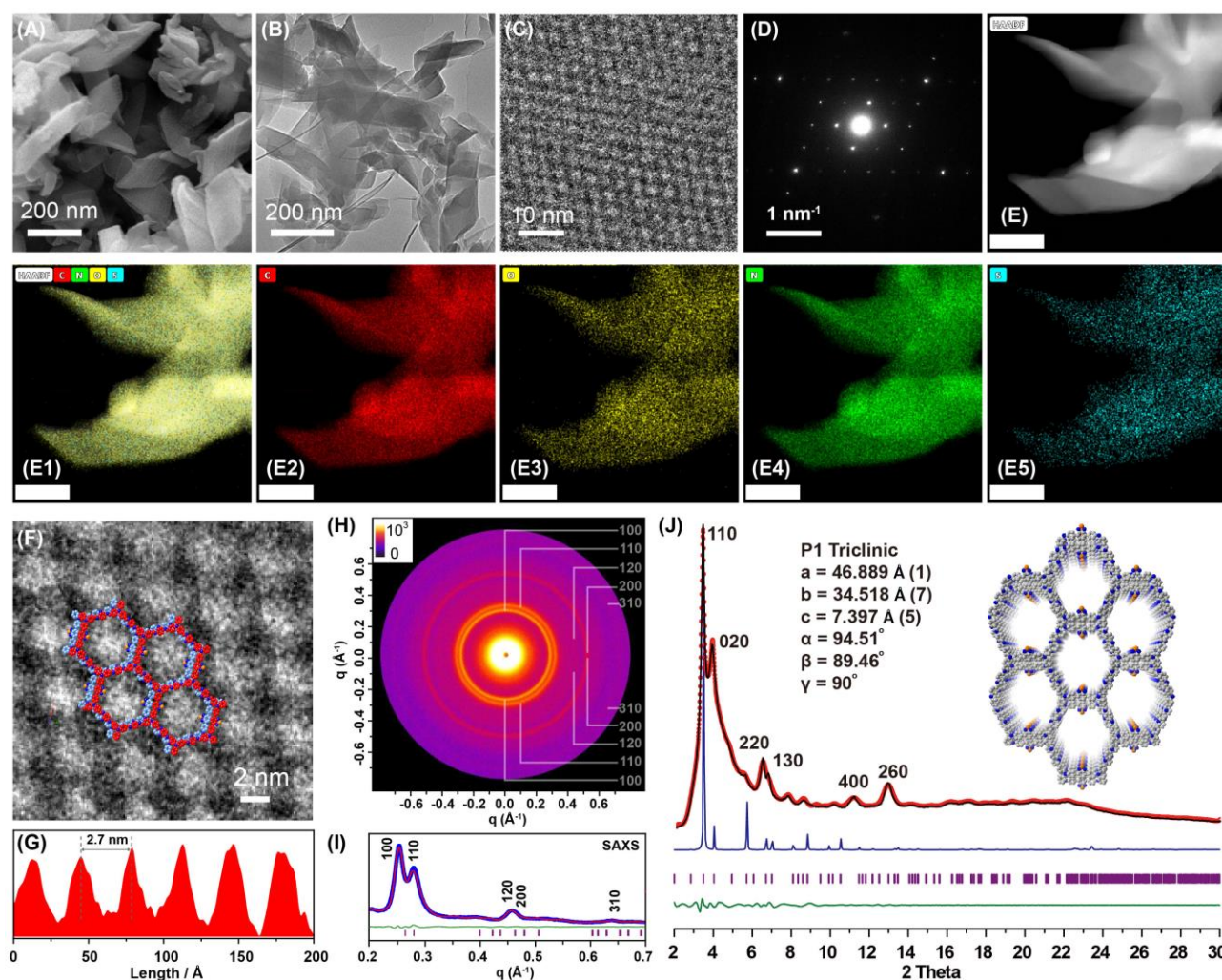


Figure 3. (A) SEM image of TPA-COF. (B) TEM image of TPA-COF. (C) Scanning TEM (STEM) image of TPA-COF under integrated differential phase contrast (iDPC) method. (D) Electron diffraction pattern of TPA-COF. (E) HAADF-STEM image and the corresponding STEM-EDS elemental mapping images of TPA-COF, scale bar = 50 nm (E1, merge; E2, C; E3, O; E4, N; E5, S). (F) Inverse FFT of C, which matched well with the structure solved by Pawley refinement. (G) Inverse voids changes of F. (H) Electron diffraction fringe of TPA-COF. (I) Small angle X-ray scattering (SAXS) data of TPA-COF. (J) Simultaneous Pawley refinements of experimental synchrotron data of TPA-COF, where red circles are experimental data, black line is calculated data, green line is the difference and purple bars Bragg positions ($\lambda = 1.2398 \text{ \AA}$).

The crystallinity of TPA-COF was reflected in the sharp peaks in the powder X-ray diffraction (PXRD) patterns collected using both lab-based and synchrotron X-ray source. To determine the crystal structure of TPA-COF, the model was built on the basis of the possible linkages between aldehyde chromophores and aniline building blocks and with different interlayer stacking for the layered structures. Comparison between the experimental PXRD pattern with the calculated from simulated structure showed excellent match in both peak positions and intensities for the layered model with eclipsed interlayer stacking (Figure S5). The PXRD pattern was refined against simulated COF structure by Pawley refinement, where crystal lattice in *P1* space group, $a = 46.889 \text{ \AA}$, $b = 34.518 \text{ \AA}$, $c = 7.937 \text{ \AA}$ and $\alpha = 94.51^\circ$, $\beta = 89.46^\circ$, $\gamma = 90^\circ$, was observed with acceptable residues (Figure 3J). The accurate distance between

layers along the *c* axis was determined from the 001 peak at $2\theta = 22.0^\circ$ in the PXRD pattern. In addition, small angle X-ray scattering (SAXS) patterns were measured for these samples to provide accurate positions and intensities for low angle peaks (100, 110, 120, 200 and 310, etc.) (Figure 3H and 3I). The refinement for both the PXRD and SAXS patterns yielded low residues. To confirm the correct choice of space group for TPA-COF in the structure refinement, electron diffraction (ED) was taken on TPA-COF crystals using TEM. The ED pattern along the zone axis of [001] direction revealed the high crystallinity of TPA-COF and determined γ angle for the crystal lattice, which was in good accordance with that obtained from PXRD refinement (Figure 3D). Furthermore, the hexagonal pores and the close packing between the layers of TPA-COF was visualized by high resolution TEM (HR-TEM) images and

scanning TEM (STEM) images, which matched well from the structure solved by PXRD (Figure 3C). Here, we used integrated differential phase contrast (iDPC) method on the STEM model, where the intensity of the signal in the image reflects the phase transition function of TPA-COF (Figure 3F). This allowed us to achieve a resolution of 2.3 Å and directly observe the pores of

TPA-COF, with a size of 28.2 Å along [100] direction, which was also consistent with the PXRD results (Figure 3G). These results reveal that TPA-COF exhibits good crystallinity and the structural slipping of the chromophores, which is important to obtain strong fluorescence emission.^[16]

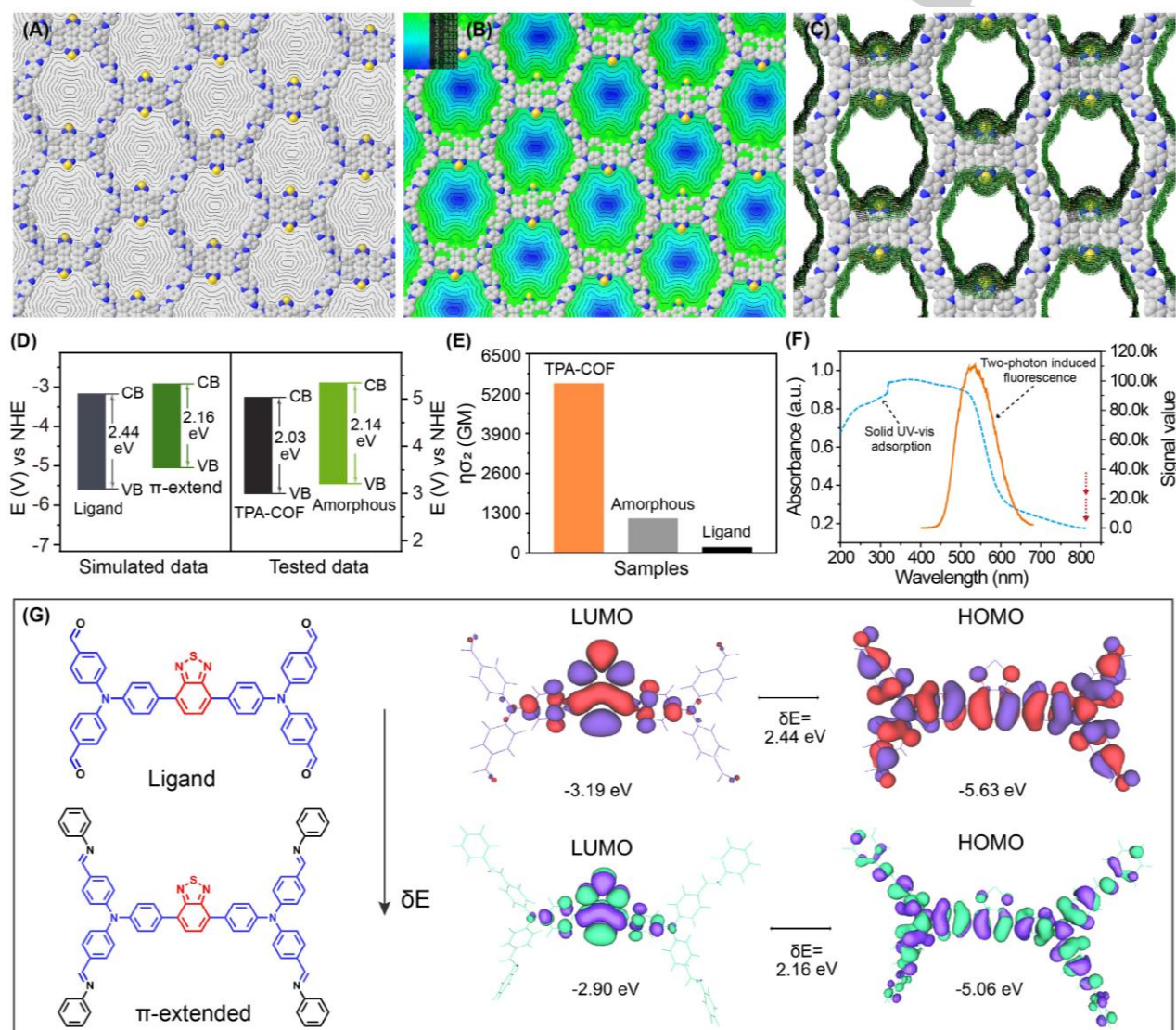


Figure 4. (A) The contours of voids in TPA-COF. (B) The contours and planes of voids in TPA-COF. (C) The surface of voids in TPA-COF. (D) Bandgap of amorphous polymer and TPA-COF (Left, simulated bandgap of ligand and π -extended ligand). (E) TPA cross-section value of the ligand and the corresponding amorphous polymer and TPA-COF. (F) UV-vis diffuse reflectance spectrum and two-photon excited emission of TPA-COF. (G) Molecular orbital amplitude plots of HOMO and LUMO of the ligand and π -extended ligand calculated at the B3LYP/6-31G (d, p) basis set.

The two-photon action cross-section was determined by using the femtosecond fluorescence measurement technique (Figure 4F). The TPA-COF was well dispersed in water with the modification of PF-127 by ultrasound and the two-photon induced fluorescence intensity was measured in the range from 760 to 860 nm by using Rhodamine B in methanol at a concentration of 1×10^{-5} M as the reference (Figure 4E). Notably,

ligand displays a TPA cross-section of 190 GM (Goeppert-Mayer unit), whereas TPA-COF show an enhanced value of 5500 GM (Rhodamine B, TPA = 70 GM, excited at 780 nm). Furthermore, TPA performance of TPA-COF was promoted drastically as the coherent domain increased. The TPA cross-section values of TPA-COF per chromophore had already doubled that of amorphous sample (1100 GM). This value rivaled that of the

state-of-the-art molecule-based TPA materials, demonstrating the power of coherent domain in TPA performance. The extension of π -conjugation is often blocked to form amorphous polymers for their polymerization reactions are irreversible and lack of an in situ structural self-healing process. To better understand two-photon excitation transitions within π -conjugation structures, we carried out density functional theory (DFT) calculations for the ligand and the corresponding π -conjugation structure. The molecular orbital density of the HOMO is primarily located on the π -conjugation moiety and the central benzothiadiazole ring, while the LUMO level is mainly localized on the acceptor framework, suggesting a significant decrease in the bandgap for the π -extended structure (Figure 4G).

Given the crystalline structure of TPA-COF, we inferred that the underlying mechanism for the promotion in TPA performance could be attributed to the restriction of the conformation dynamics, the formation of π -conjugation domain and long-range order in TPA-COF. The voids and surface of TPA-COF were calculated by Olex 2, indicating the structural slipping in the crystal structure (Figure 4A-4C). The layered eclipsed stacking configuration imposed by the triarylamine unit in TPA-COF restricted the conformation dynamics. Here, this not only increased the crystallinity of TPA-COF, but also reduced the unwanted non-radiative energy decay during the TPA process. Furthermore, the impact of π -conjugation domain was further investigated by spectroscopic studies. The band gap was measured by UV-vis diffuse reflectance spectroscopic (DRS), while the valence band was given by ultraviolet photoelectron spectroscopic (UPS) collected using XPS instrument, therefore revealing the accurate band structure of TPA-COF (Figure 4F and S6). In comparison to the corresponding molecular building blocks, TPA-COF exhibited lower fluorescence lifetime, excellent photo-stability and wide range of excitation (Figure S6-S10). This combined with the red shift in the UV-vis absorption spectrum confirmed the cooperation between chromophores across the entire COF crystals (Figure 5B). The interaction between chromophores at different layers along *c* axis of the crystal lattice was reflected in the chemical shift of the carbon on the triarylamine motif after the formation of COF, where the rotation freedom of the aryl group was restricted. The differences in π -conjugation domain were further reflected in their optical properties. As the coherent domain increased, the one-photon fluorescence intensity of TPA-COF enhanced drastically, while the band gap decreased from 2.52, 2.14 to 2.03 eV for the ligand, amorphous polymer and long-range crystal, respectively (Figure 4D, S11 and S12).

Inspiring the efficient two-photon absorption of TPA-COF, we further investigated the two-photon fluorescence imaging and biosafety of TPA-COF *in vitro*. Dynamic light scattering (DLS) measurements on TPA-COF gave the zeta potential of -13.4 mV and an average diameter of 345 nm with a polydispersity index (PDI) of 0.189 (Figure 5A). We found that the size and zeta potential of TPA-COF showed no obvious changes in 72 h, indicating the stability at the physiological condition. As shown in

Figure S13, when TPA-COF were treated with PBS solution (50 mM) for 12 and 24 h, PXRD patterns have no obvious change. This result indicates that TPA-COF exhibited good structure stability. To assess the biosafety of the TPA-COF, the established methyl thiazolyl tetrazolium (MTT) assay was carried out on the normal (3T3) and cancer (4T1) cells line in the dark or with 808 nm laser irradiation (Figure 5C and 5D). Moreover, TPA-COF showed good biocompatibility with over 90% cell viability when incubated with cells alone. The decrease in cell viability in Figure 5C and 5D could be attributed to weak photo-thermal effect of TPA-COF under laser irradiation (Figure S14 and S15). Notably, the cells could well survive when treated with 250 μ g/mL of TPA-COF upon 808 nm laser irradiation.

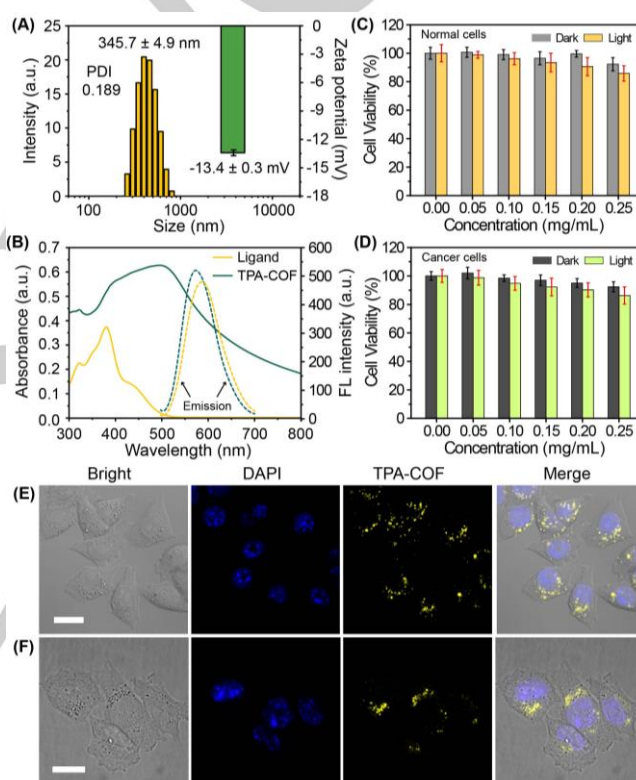


Figure 5. (A) Particle size and zeta potential of TPA-COF. (B) UV-vis and fluorescence spectrum of TPA-COF. (C) The cytotoxicity of TPA-COF against normal cells. (D) The cytotoxicity of TPA-COF against cancer cells. (E) Two-photon fluorescence imaging of TPA-COF against 4T1 cells. (F) One-photon fluorescence imaging of TPA-COF against 4T1 cells. Scale bar, 50 μ m.

The intracellular distribution and uptake of TPA-COF were confirmed by two-photon confocal laser scanning microscopy (CLSM) in 4T1 cell line. It was found that obvious yellow fluorescent signal from the endocytosis of TPA-COF was observed through CLSM upon two-photon excitation with an 810 nm laser, indicating that TPA-COF exhibited efficient two-photon fluorescence and could be internalized within 4T1 cells (Figure 5E). Compared with one-photon excitation fluorescence imaging, two-photon excitation exhibits high focal spot and resolution

(Figure 5F). The z-stack confocal images were taken continuously from the bottom to the top via two-photon laser confocal scanning microscopy (TPLCSM). The image stacks were processed by Image J software to obtain the 3D reconstruction movie of 4T1 cell. Intense intracellular luminescence was observed with femtosecond laser pulses at 810 nm, under which no background fluorescence from the 4T1 cells would interfere (Figure S16). Benefiting from the high TPA cross-section value of TPA-COF, high signal strength can be obtained. The large TPA cross-section and high photostability of TPA-COF make it a good candidate for *in vivo* TPLCSM imaging.

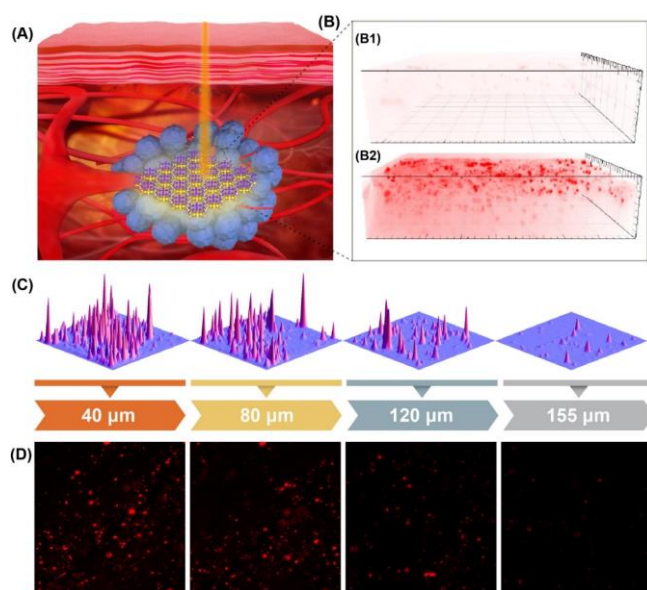


Figure 6. (A) Schematic illustrating TPA-COF for tumor imaging *in vivo*. (B) The two-photon excited fluorescence imaging of TPA-COF at 4T1 tumor xenograft in Balb/c mice model (B1, PBS group; B2, TPA-COF group). (C) The two-photon fluorescence intensity of TPA-COF at different tumor tissue depth. (D) The two-photon fluorescence imaging of TPA-COF at different tumor tissue depth.

To evidence the feasibility of TPA-COF *in vivo*, 4T1 tumor xenograft in Balb/c mice model was established for evaluating the bio-distribution of TPA-COF on a small animal imaging system. The two-photon fluorescence imaging was measured by two-photon electrophysiological microscope (OLYMPUS, FV1200) after intravenous injection of TPA-COF (Figure 6A). Considering that the nanoparticles tend to accumulate in tumor tissue through enhanced permeability and retention (EPR) effect during *in vivo* circulation.^[17] As shown in Figure 6B, very bright dot-like fluorescent signal was observed with almost no background in tumor tissue under 810 nm two-photon excitation. Taking advantage of the two-photon excitation, Figure 6C and 6D show the images of TPA-COF at different depths with the maximum detectable depth up to around 150 μm . Compared with one-photon excitation, two-photon excitation exhibits deeper tissue penetration (Figure S17). These results also reveal the great potential of TPA-COF serve as one- and two-

photon bio-probes for studying the biological processes in cells, tissues, and mouse models.

Conclusion

In summary, we have demonstrated that TPA-COF could work as a promising candidate with efficient TPA performance by utilizing the unique crystalline feature of COF. It is worth noting that TPA-COF exhibiting the slipped structure between the layers, the long-range crystal domain, and the π -conjugation domain of the corresponding monomer greatly improves the delocalization of π -electrons, which lead to high dipole value and TPA activity. When the crystalline feature was accessed, the formation of COFs led to significant improvement in the TPA cross-section value per chromophore (the increase of 30.0-fold, 5.0-fold compared with ligand and amorphous polymer, respectively), already surpassing those achieved by traditional methods such as molecular design and polymerization. Furthermore, upon the TPA efficiency, the TPA-COF can be used as enhanced imaging agents for *in vitro* and *in vivo* two-photon fluorescence imaging. We expect that this work will offer a pathway to overcome aggregation-caused quenching and acquire near-infrared two-photon excited COFs for future biomedical applications.

Acknowledgements

This work was financially supported by the National Natural Science Foundation of China (51903191, 51833007, 21721005 and 51690152) and China Postdoctoral Science Foundation (Nos. 2019TQ234 and 2019M652693). We thank L. Zhang, H. Deng (Wuhan University) for their invaluable help and discussion. All of the animal experiments were conducted under protocols approved by the Institutional Animal Care and Use Committee (IACUC) of the Animal Experiment Center of Wuhan University (Wuhan, China).

Conflict of interest

The authors declare no conflict of interest.

Keywords: covalent organic framework • slipped structure • long-range order • two-photon absorption • fluorescence imaging

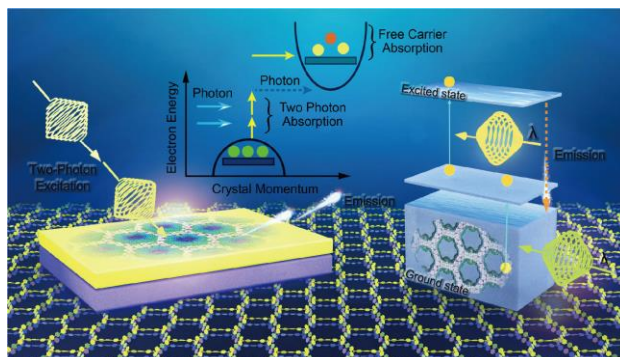
- [1] J. Jiang, Y. Zhao, O. M. Yaghi, *J. Am. Chem. Soc.* **2016**, *138*, 3255-3265.
- [2] P. J. Waller, F. Gándara, O. M. Yaghi, *Acc. Chem. Res.* **2015**, *48*, 3053-3063.
- [3] C. S. Diercks, O. M. Yaghi, *Science* **2017**, *355*, eaal1585.
- [4] a) S. Lin, C. S. Diercks, Y. B. Zhang, N. Kornienko, E. M. Nichols, Y. Zhao, A. R. Paris, D. Kim, P. Yang, O. M. Yaghi, C. J. Chang, *Science* **2015**, *349*, 1208-1213; b) S. Ding, J. Gao, Q. Wang, Y. Zhang, W. Song, C. Su, W. Wang, *J. Am. Chem. Soc.* **2011**, *133*, 19816-19822; c) H. Xu, J. Gao, D. Jiang, *Nat. Chem.* **2015**, *7*, 905; d) C. J. Doonan, D. J. Tranchemontagne, T. G. Glover, J. R. Hunt, O. M. Yaghi, *Nat. Chem.* **2010**, *2*, 235; e) S. Ding, M. Dong, Y. Wang, Y. Chen, H. Wang, C. Su,

- W. Wang, *J. Am. Chem. Soc.* **2016**, *138*, 3031-3037; f) H. Qian, C. Yang, X. Yan, *Nat. Commun.* **2016**, *7*, 12104.
- [5] a) E. Jin, M. Asada, Q. Xu, S. Dalapati, M. A. Addicoat, M. A. Bragy, H. Xu, T. Nakamura, T. Heine, Q. Chen, D. Jiang, *Science* **2017**, *357*, 673-676; b) X. Li, Q. Gao, J. Wang, Y. Chen, Z. Chen, H. Xu, W. Tang, K. Leng, G. Ning, J. Wu, Q. Xu, S. Y. Quek, Y. Lu, K. P. Loh, *Nat. Commun.* **2018**, *9*, 2335.
- [6] a) M. J. Miller, S. H. Wei, I. Parker, M. D. Cahalan, *Science* **2002**, *296*, 1869-1873; b) D. R. Larson, W. R. Zipfel, R. M. Williams, S. W. Clark, M. P. Bruchez, F. W. Wise, W. W. Webb, *Science* **2003**, *300*, 1434-1436; c) S. Krol, R. Macrez, F., Docagne, G. Defers, S. Laurent, M. Rahman, M. J. Hajjipour, P. G. Kehoe, M. Matmoudi, *Chem. Rev.* **2012**, *11*, 1877-1903; d) J. P. Celli, B. Q. Spring, I. Rizvi, C. L. Evans, K. S. Samkoe, S. Verma, B. W. Pogue, T. Hasan, *Chem. Rev.* **2010**, *110*, 2795-2838; e) I. Medintz, H. T. Uyeda, E. R. Goldman, H. Mattoussi, *Nat. Mater.* **2005**, *4*, 435; f) M. Q. Zhu, G. F. Zhang, C. Li, M. P. Ardrred, E. Chang, R. A. Drezek, A. D. Q. Li, *J. Am. Chem. Soc.* **2010**, *133*, 365-372; g) L. Ji, S. Griesbeck, T. B. Marder, *Chem. Sci.* **2017**, *8*, 846-863.
- [7] a) H. M. Kim, B. R. Cho, *Chem. Rev.* **2015**, *115*, 5014-5055; b) F. Bolze, S. Jenni, A. Sour, V. Heitz, *Chem. Commun.* **2017**, *53*, 12857-12877.
- [8] M. Albota, D. Beljonne, J. L. Bredas, J. E. Ehrlich, J. Y. Fu, A. A. Heikal, S. E. Hess, T. Kogej, M. D. Levin, S. R. Marder, D. McCord-Maughon, J. W. Perry, H. Rockel, M. Rumi, G. Subramaniam, W. W. Webb, X. L. Wu, C. Xu, *Science* **1998**, *281*, 1653-1656.
- [9] a) F. Terenziani, C. Katan, E. Badaeva, S. Tretiak, M. Blanchard-Desce, *Adv. Mater.* **2008**, *20*, 4641-4678; b) Y. Jin, Y. Hu, W. Zhang, *Nat. Rev. Chem.* **2017**, *1*, 1; c) S. Y. Ding, W. Wang, *Chem. Soc. Rev.* **2013**, *42*, 548-568; d) R. Medishetty, L. Nemeč, V. Nalla, S. Henke, M. Samoc, K. Reuter, R. A. Fischer, *Angew. Chem. Int. Ed.* **2017**, *56*, 14743-14748.
- [10] a) S. Kim, Q. Zheng, G. S. He, D. J. Bharali, H. E. Pudavar, A. Baev, P. N. Prasad, *Adv. Funct. Mater.* **2006**, *16*, 2317-2323; b) G. S. He, L. S. Tan, Q. D. Zheng, P. N. Prasad, *Chem. Rev.* **2008**, *108*, 1245-1330.
- [11] a) R. Medishetty, J. K. Zareba, D. Mayer, Marek. Samoc, R. A. Fischer, *Chem. Soc. Rev.* **2017**, *46*, 4976-5004; b) E. Collini, C. Ferrante, R. Bozio, A. Lodi, G. Ponterini, *J. Mater. Chem.* **2006**, *16*, 1573-1578; c) G. P. Bartholomew, M. Rumi, S. J. K. Pond, J. W. Perry, S. Tretiak, G. C. Bazan, *J. Am. Chem. Soc.* **2004**, *126*, 11529-11542; d) J. Y. Zeng, M. Z. Zou, M. K. Zhang, X. S. Wang, X. Zeng, H. Cong, X. Z. Zhang, *ACS Nano* **2018**, *12*, 4630-4640; e) J. Y. Zeng, X. S. Wang, W. F. Song, H. Cheng, X. Z. Zhang, *Adv. Therap.* **2019**, *2*, 1800100.
- [12] a) N. Huang, P. Wang, D. Jiang, *Nat. Rev. Mater.* **2016**, *1*, 16068; b) A. P. Cote, A. I. Benin, N. W. Ockwig, M. O'Keeffe, A. J. Matzger, O. M. Yaghi, *Science* **2005**, *310*, 1166-1170; c) X. Feng, X. Ding, D. Jiang, *Chem. Soc. Rev.* **2012**, *41*, 6010-6022; d) J. L. Segura, M. J. Mancheno, F. Zamora, *Chem. Soc. Rev.* **2016**, *45*, 5635-5671.
- [13] Y. Zhou, F. Meng, X. Zhao, S. Feng, M. Jiang, *Chem. Phys.* **2001**, *269*, 441-445.
- [14] a) T. Ishi-i, N. Nakamura, S. Amemori, K. Kasatani, H. Gorohmaru, M. Ishida, M. Shigeiwa, *Dyes. Pigments* **2013**, *99*, 14-19; b) Z. Zhao, P. Lu, J. W. Y. Lam, Z. Wang, C. Y. K. Chan, H. H. Y. Sung, I. D. Williams, Y. Ma, B. Z. Tang, *Chem. Sci.* **2011**, *2*, 672-675.
- [15] a) M. Pawlicki, H. A. Collins, R. G. Denning, H. L. Anderson, *Angew. Chem. Int. Ed.* **2009**, *48*, 3244-3266; b) L. Ascherl, T. Sick, J. T. Margral, S. H. Lapidus, M. Calik, C. Hettstedt, K. Karaghiosoff, M. Doblinger, T. Clark, K. W. Chapman, F. Auras, T. Bein, *Nat. Chem.* **2016**, *8*, 310; c) J. Y. Zeng, M. K. Zhang, M. Y. Peng, D. Gong, X. Z. Zhang, *Adv. Funct. Mater.* **2018**, *28*, 1705451; d) J. Y. Zeng, X. S. Wang, Y. D. Qi, Y. Yu, X. Zeng, X. Z. Zhang, *Angew. Chem. Int. Ed.* **2019**, *131*, 5748-5752.
- [16] a) M. M. Alam, M. Chattopadhyaya, S. Chakrabarti, K. Ruud, *Acc. Chem. Res.* **2014**, *47*, 1604-1612; b) L. Sun, W. Zhu, W. Wang, F. Yang, C. Zhang, S. Wang, X. Zhang, R. Li, H. Dong, W. Hu, *Angew. Chem. Int. Ed.* **2017**, *56*, 7831-7835.
- [17] a) C. L. Sun, J. Li, X. Z. Wang, R. Shen, S. Liu, J. Q. Jiang, T. Li, Q. W. Song, Q. Liao, H. B. Fu, J. N. Yao, H. L. Zhang, *Chem* **2019**, *5*, 600-616; b) Z. Zheng, T. Zhang, H. Liu, Y. Chen, R. T. K. Kwok, C. Ma, P. Zhang, H. H. Y. Sung, I. D. Williams, J. W. Y. Lam, K. S. Wong, B. Z. Tang, *ACS Nano* **2018**, *12*, 8145-8159; c) H. Cao, L. Wang, Y. Yang, J. Li, Y. Qi, Y. Li, Y. Li, H. Wang, J. Li, *Angew. Chem. Int. Ed.* **2018**, *57*, 7759-7763.

Table of Contents

RESEARCH ARTICLE

A benzothiadiazole-based covalent organic framework with slipped structure was reported to promote the two-photon adsorption performance and overcome the aggregation-caused emission quenching of the chromophores for improving near-infrared two-photon excited fluorescence imaging.



Jin-Yue Zeng, Xiao-Shuang Wang, Bo-Ru Xie, Min-Jie Li, and Xian-Zheng Zhang*

Page No. – Page No.

Slipped Structure of Covalent Organic Framework Facilitates Two-Photon Adsorption for Improving Near-Infrared Excited Fluorescence Imaging